Supporting information

Macromolecular Electrolyte Engineering for Tuning Zn-Ion Solvation Chemistry and Boosting H^+ Storage toward Stable Aqueous Zinc-Organic Batteries

Linqi Cheng‡[,a,b] Mengfan Li‡[,b] Xupeng Zhang‡[,b] Wanting Wang,[a] Lina Zhao,[a,c,*] and Heng-Guo Wang*[,b]

[a]Key Laboratory of Preparation and Applications of Environment Friendly Materials, Ministry of Education, Jilin Normal University, Changchun 130103, P. R. China

[b]Key Laboratory of Polyoxometalate and Reticular Material Chemistry of Ministry of Education, Faculty of Chemistry, Northeast Normal University, Changchun 130024, P. R. China.

[c]College of Chemistry, Jilin Normal University, Siping, 136000, P. R. China.

[+]These authors contributed equally to this work.

Email: zhaolina1975@jlnu.edu.cn (L. Zhao); wanghengguo@cust.edu.cn (H. Wang)

Contents

Section 1. Materials and Synthetic Procedures

1.1 Materials

Tetrachloro-p-benzoquinone (Macklin, 98%), potassium phthalimide (Macklin, 98.0%), 2,5-dihydroxy-1,4-benzoquinone (DHBQ, Aladdin, 98%), hydrazine hydrate (Aladdin, 80.0wt%), zinc trifluoromethanesulfonate (Aladdin, 98%), Tetra(phthalimido)-benzoquinone (TPB, Aladdin, 98%), Zn foils (purity 99.99%), zinc sulfate heptahydrate ($ZnSO_4 \cdot 7H_2O$, Sigma-Aldrich, 99%), *N*-methyl pyrrolidone (NMP, Aladdin, 99.5%), acetonitrile (Aladdin, >99.5%, AR), 4,4′,4″,4‴-(porphine-5,10,15,20-tetrayl)tetrakis(benzenesulfonic acid) (TPPS, Jilin Chinese Academy of Sciences Yanshen Technology Co., Ltd, 95%), meso-tetra(4-carboxyphenyl)porphine (TCPP, Jilin Chinese Academy of Sciences Yanshen Technology Co., Ltd, 98%), 5,10,15,20-tetrakis(4-aminophenyl)-21H,23H-porphine (TAPP, Jilin Chinese Academy of Sciences Yanshen Technology Co., Ltd, 98%), 5,10,15,20-tetrakis(pentafluorophenyl)-21H,23H-porphine (TPPP, Jilin Chinese Academy of Sciences Yanshen Technology Co., Ltd, 98%), hydrochloric acid, anhydrous ethanol, acetone and anhydrous methanol were purchased and used without further purification.

1.2 Synthetic Procedures

Synthesis of TABQ: TABQ was synthesized according to the literature.[S1] 3.39 g tetrechloro-p-benzoquinone was dispersed in 150 mL anhydrous acetonitrile and 9.94 g potassium phthalimide was added into the mixture under N_2 atmosphere with stirred for 12 h at 80 °C. The mixture was filtered after cooling down to room temperature. Then, the filtered solid was washed by DMF and deionized water. The product was further washed with deionized water several times until the filter liquor was colorless. TPB was obtained after dried at 80 °C in vacuum overnight. Further, 10 mL hydrazine hydrate (85.0 wt%) was added slowly into a round bottom flask containing TPB (1.0

g). The mixture was stirred at 65 °C for 6 h. After cooling down to room temperature, the mixture was filtered and washed with plenty of deionized water. Finally, TABQ was obtained and dried at 80 °C in vacuum overnight.

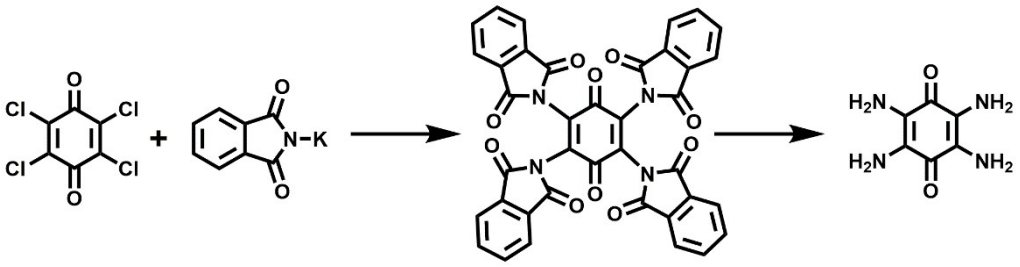

Scheme S1. Synthetic route of TABQ.

Synthesis of QAP: QAP was synthesized according to the literature.[S2] The mixture of DHBQ (1.05 g, 7.5 mmol), TABQ (0.25 g, 1.5 mmol) and acetic acid (10 mL) were added into a round-bottom flask and then refluxed at 140 °C for 48 h under N_2. After cooling to room temperature, the black reaction mixture was filtered and washed with HCl, water, MeOH and acetone until the filtrate was clear, and then dried in vacuum at 80 °C overnight to yield the black powder.

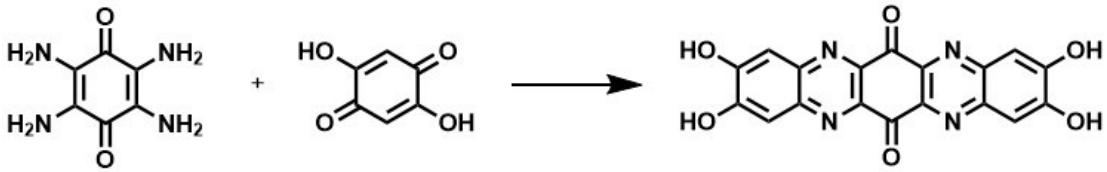

Scheme S2. Synthetic route of QAP.

1.3 Characterizations

Scanning electron microscopy (SEM) images were performed by HITACHI SU8010. Powder X-ray diffraction (XRD) measurements were tested on Smartlab (Cu Kα-radiation, λ=0.15405 nm, 40 kV, 30 mA). Fourier transformed infrared (FT-IR) spectra were determined by TJ270-30A. ICP-AES (LEEMAN, American) was performed to analyze Zn and S content. The ^{1}H NMR spectra were determined by 500MHz Nuclear Magnetic Resonance Spectrometer (Avance NEO 500). The surface

roughness of the electrode was tested with an atomic force microscope (AFM) (Asylum MFP3D). The chemical state of Zn anode in the different electrolytes was analyzed by using the X-ray photoelectron spectroscopy (XPS, ESCALAB 250, Thermo) with Al Kα radiation and energy step size of 1 eV. The contact angles of electrolytes on the Zn foil were tested by using the static contact angle measurements (sl200kb, Kino, USA).

Section 2. Theory Calculation

2.1 DFT computational details

All geometry structures were optimized using Gaussian 16 software package under B3LYP/6-31G (d, p) /UB3LYP level of theory followed by vibrational frequency calculations and to further confirm their stability.[S3] The binding energy (ΔE) of H^+ and Zn^{2+} with the molecule was calculated by the following formula:

$$\Delta E = (E_{xZn/H}-E_{(x-1)Zn/H}-E_{Zn/H})$$

Where $E_{xZn/H}$ and $E_{(x-1)Zn/H}$ represent the total energy of the final and initial states of the zinc inserting, $E_{Zn/H}$ is the total energy of Zn/H.

2.2 COMSOL Multiphysics

The electric field distribution and Zn^{2+} ion flux at the electrode-electrolyte interface were simulated using COMSOL Multiphysics software. The simulations were performed using the Butler-Volmer expression to describe the reaction kinetics at all electrodes, and the flux of each ion was calculated by the Nernst-Planck equation. The model the processed electrochemistry model was imported into the finite element software COMSOL® (Stockholm, Sweden), where the material properties were defined and the relevant problems were calculated and analyzed. To solve the discretized transport and electrode deformation kinematics equations, the Parallel Direct Sparse Solver (PARDISO) was employed. Time stepping was handled using

2nd order backward Euler differentiation.

2.3 Molecular dynamics (MD) simulations

All of the 0.8 scale OPLS-AA force field parameters of ions used in this work were obtained from previous report.[S4] The small molecules (water, TSPP, $ZnSO_4$) were reasonably optimized via Gaussian 16 software with a level of B3LYP/def2tzvp before simulations.[S5] The OPLS-AA force field parameters of them were obtained from Ligpargen web server. Moreover, the RESP2 charge were used for obtaining more accurate results. The initial structures were modelled via Packing Optimization for Molecular Dynamics Simulations (Packmol) program and the periodic box was set to 100×100×100 $Å^3$. Besides, the time step was fixed to be 1 fs. The electrolyte systems were equilibrated in the isothermal-isobaric ensemble (constant NPT) using the Berendsen barostat to maintain the pressure of 1 GPa with 10 ns. Then, the productions run of 10 ns were then obtained in the canonical ensemble (NVT) at 298 K. The simulation time was long enough to ensure reaching the equilibrium states of the electrolyte systems.

2.4 DFT calculation details

Vienna ab initio simulation package (VASP) [S6,S7] was employed to perform all density functional theory (DFT) calculations within the generalized gradient approximation (GGA), which uses the Perdew-Burke-Ernzerhof (PBE) [S8] formulation. We have selected the projected augmented wave (PAW) potentials [S9,S10] to describe the ionic cores. Additionally, we take valence electrons into account using a plane wave basis set with a kinetic energy cutoff of 400 eV. Partial occupancies of the Kohn-Sham orbitals were allowed under the occasion which uses the Gaussian smearing method and a width of 0.05 eV. The electronic energy can be considered self-consistent if the energy change was smaller than 5-10 eV. When the force change

is less than 0.05 eV/Å, the geometric optimization is considered to converge. The dispersion interactions were described by Grimme's DFT-D3 methodology [S11]. The Brillourin zone was sampled with a gamma-centered grid 1×1×10 through all computational process[S12]. The solvation environment was considered by applying the implicit solvation model VASP sol [S13, S14], which is based on solving the linearized Poisson Boltzmann equation. The adsorption energy (Eads) of adsorbate A was defined as following formula:

$$E_{ads} = E_{A/surf} - E_{surf} - E_{A(g)}$$

where $E_{A/surf}$, E_{surf} and $E_{A(g)}$ are corresponding to the energy of adsorbate A adsorbed on the surface, the energy of clean surface, and the energy of isolated A molecule in a cubic periodic box, respectively.

Section 3. Electrochemical Measurements

3.1 Electrolyte preparation

2 M $ZnSO_4$ electrolyte was prepared by dissolving $ZnSO_4 \cdot 7H_2O$ in deionized water. Different amounts of TPPS (2, 4, 6 and 8 mg, which were denoted as TPPS-2, TPPS-4) TPPS-6, and TPPS-8) were added into 1 mL of 2 M $ZnSO_4$ electrolyte, respectively. Control electrolytes (TAPP/$ZnSO_4$, TCPP/$ZnSO_4$ and TPPP/$ZnSO_4$ electrolytes) were prepared using the similar step except adding different porphyrin additives.

3.2 Electrochemical test

All cells were fabricated based on CR2025-typed coin cells with LAND test system to measure the electrochemical performances. Before assembling the cells, Zn foil was stamped into disks with a diameter of 12 mm. The symmetric cells were composed of two Zn foil separated with glassfiber separators, and 2 M $ZnSO_4$ and 2 M $ZnSO_4$ + TPPS-4 aqueous solution as the electrolyte in the half-cell and full cells, respectively. CA was performed by using Zn||Zn symmetric cells at a constant

overpotential of -150 mV within 300 s. The hydrogen evolution reaction was tested by using LSV method at a scan rate of 1 mV s^{-1} and a scan range from -1.9 to -1.3 V in the different electrolytes, which uses three-electrode configuration employing Pt foil as the working and counter electrodes and saturated Ag/AgCl electrode as reference electrode. Tafel plots was tested between -0.8 and -1.2 V (versus saturated Ag/AgCl electrode) at a scan rate of 1 mV s^{-1}. The current density and corrosion potential were calculated by CHI660E electrochemical workstation. Furthermore, the transparent symmetric cells of Zn anode in the different electrolytes were assembled to observe the surface morphology evolution by *in-situ* optical microscope. Electrochemical impedance spectroscopy (EIS) of all samples were measured at a fixed overpotential of 5 mV within a frequent range from 0.01 Hz to 1 MHz.

For assembling full cells, the slurry was composed of active material of QAP, acetylene black and polyvinylidene fluoride (PVDF) at the weight ratio of 4:5:1, in which NMP as the dispersants and casted onto stainless steel mesh. Subsequently, the obtained electrodes were dried in a vacuum oven under 80 ℃ for 12 h. The mass loading was about 1.0 mg cm^{-2}. The electrolyte was 2 M $ZnSO_4$ or 2 M $ZnSO_4$ + TPPS-4 (80 μL). The full cells were tested within a voltage from 0.2 to 1.4 V.

For assembling pouch cells, the electrode pellet was prepared by casting the mixture of 40 wt% QAP, 50 wt% acetylene black and 10 wt% PVDF in anhydrous NMP onto stainless steel mesh and the load of the active material is 0.4-0.5 mg cm^{-2} (the electrode is around 2.0 cm × 4.0 cm). Next, 2 M $ZnSO_4$ or 2 M $ZnSO_4$ + TPPS-4 was used as electrolyte and fiberglass was used as the separator. The voltage range was 0.2 to 1.4 V.

Section 4. Highlights of TPPS additive

Table S1. Comparison of different additives.

Additive material	Current density (mA cm^{-2})	Time (h)	Cathode material	Ref.
D-trehalose dehydrate (DT)	2	650	N, P co-doped hard carbon (NPHC)	**29**
Sodium dodecyl benzene sulfonate (SDBS)	0.5	600	$LiFePO_4$ (LFP)	**30**
Cyclodextrins	5	200	V_2O_5	**31**
Glutamine (Gln)	1	700	$NH_4V_4O_{10}$	**32**
N-methyl-2-pyr-rolidone (NMP)	1	600	VS_2@SS	**33**
Tetraphenylporphyrin tetrasulfonic acid (TPPS)	5	800	Quinone-fused aza-phenazine (QAP)	**This work**

Section 5. Analysis and Discussion

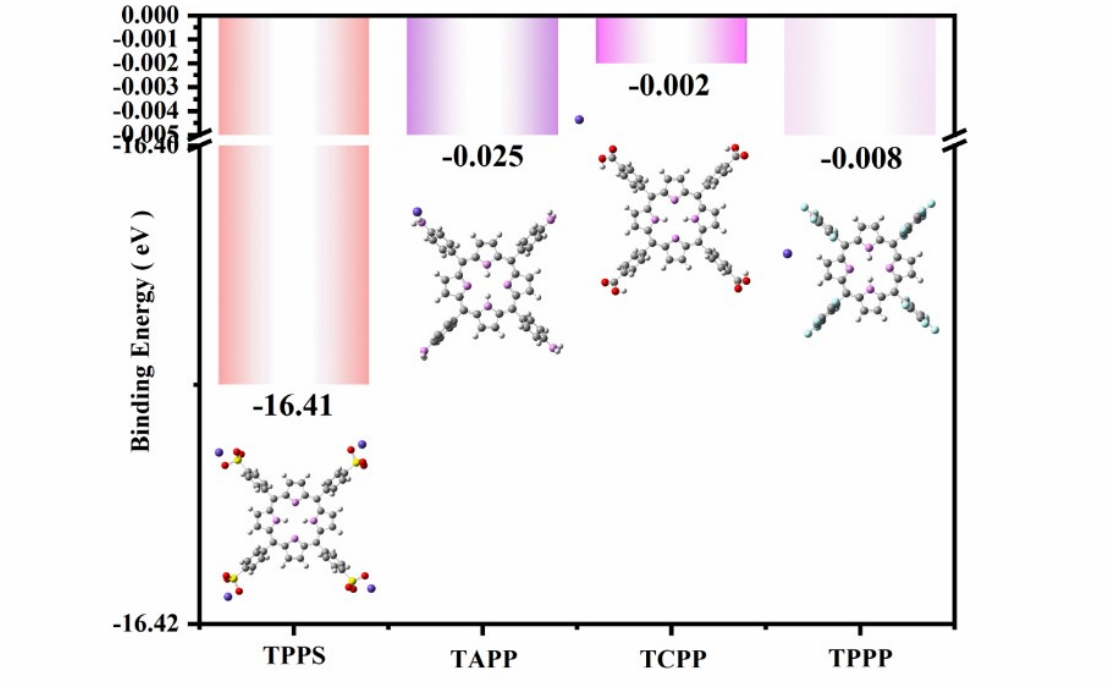

Fig. S1. Binding energies between Zn^{2+} and peripheral substituents of different porphyrin additives.

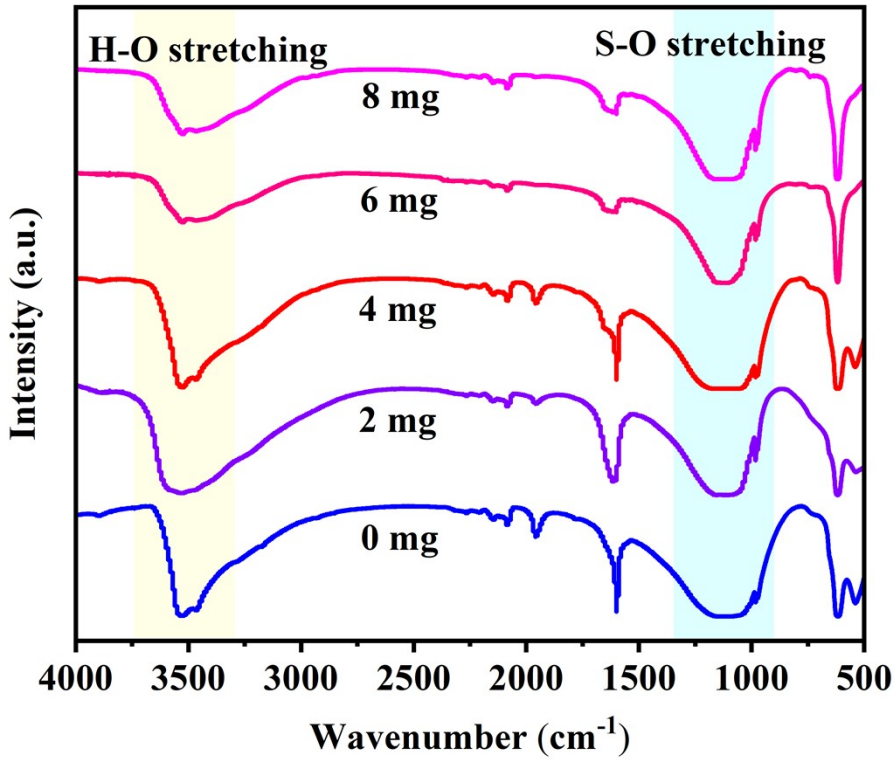

Fig. S2. FT-IR spectra of 2 M $ZnSO_4$ with TPPS-2, TPPS-4, TPPS-6 and TPPS-8.

Fig. S3. Digital photos of 2 M $ZnSO_4$ + TPPS-2, TPPS-4, TPPS-6 and TPPS-8, respectively.

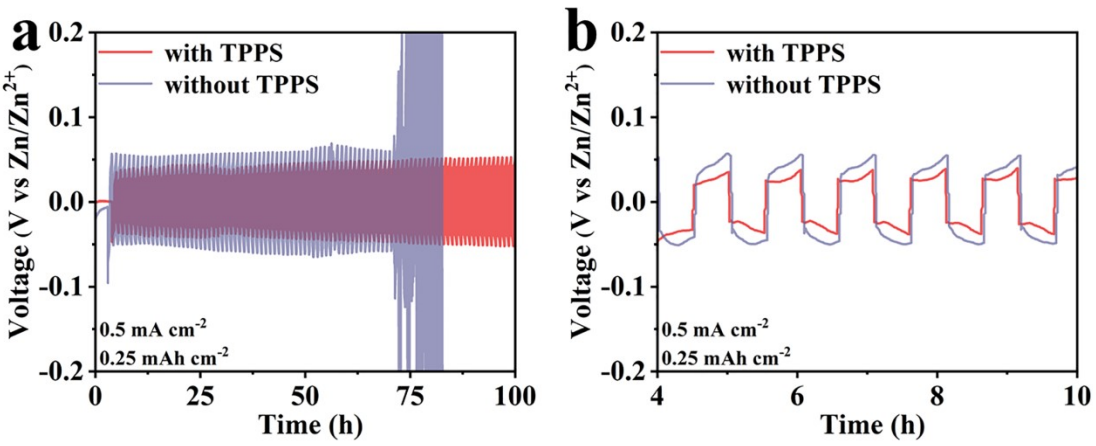

Fig. S4. Long-term cycling performance of Zn||Zn symmetric cells in different electrolytes (a) 0-100 h. (b) 4-10 h.

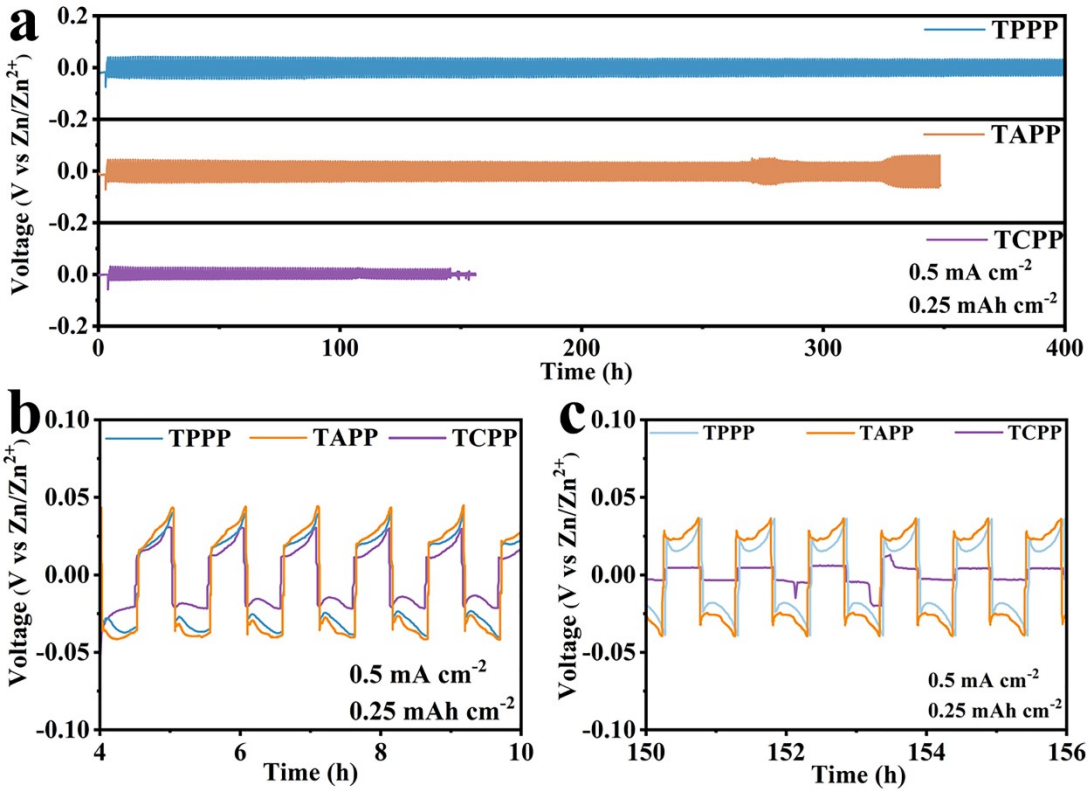

Fig. S5. (a) Long-term cycling performance of Zn||Zn symmetric cells in different electrolytes. Cyclic plating/stripping profiles at (b) 4-10 h and (c) 150-156 h.

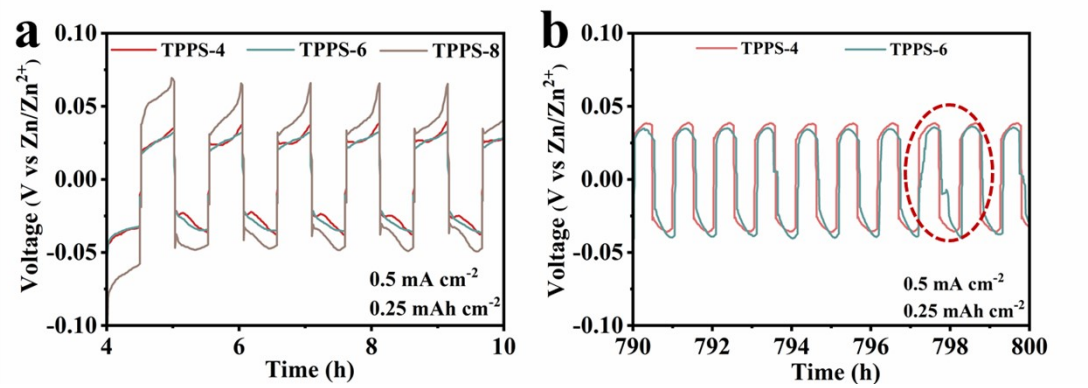

Fig. S6. Long-term cycling performance of Zn||Zn symmetric cells in different electrolytes. Cyclic plating/stripping profiles at (a) 4-10 h and (b) 790-800 h.

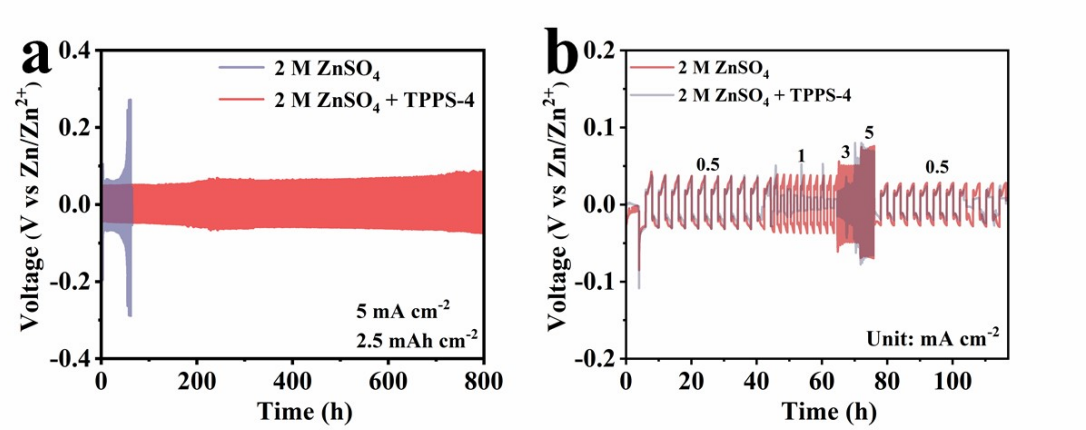

Fig. S7. (a) Long-term cycling performance of the Zn||Zn symmetric cells in 2 M $ZnSO_4$ and 2 M $ZnSO_4$ + TPPS-4 at 5 mA cm^{-2}. (b) Rate performance of the Zn||Zn symmetric cells in 2 M $ZnSO_4$ and 2 M $ZnSO_4$ + TPPS-4.

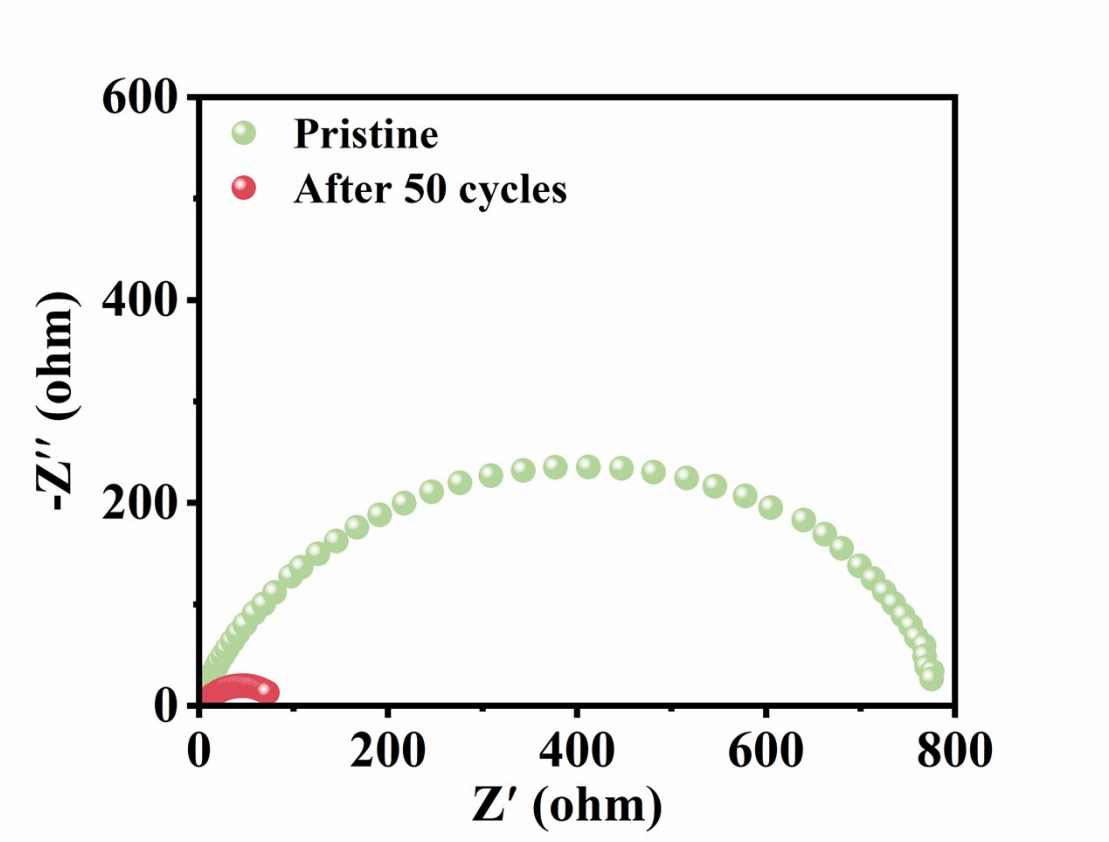

Fig. S8. EIS profiles of Zn||Zn symmetric cell in 2 M $ZnSO_4$ + TPPS-4 before and after cycling.

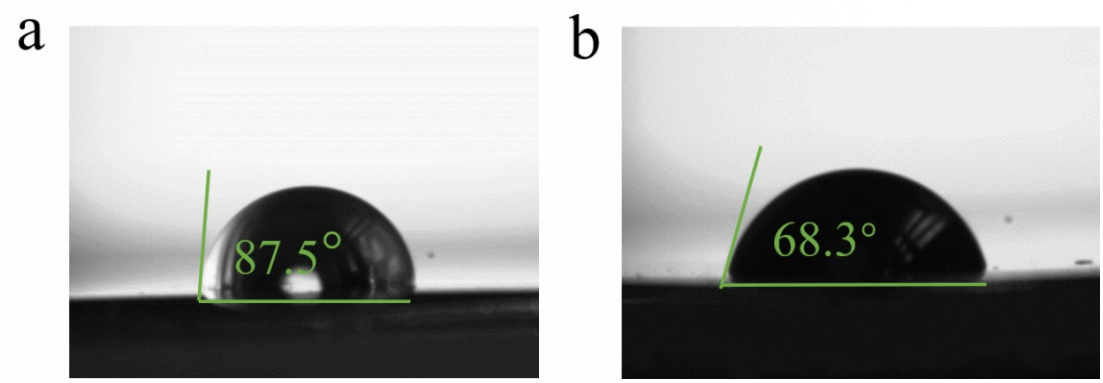

Fig. S9. Contact angles of (a) 2 M $ZnSO_4$ and (b) 2 M $ZnSO_4$ + TPPS-4 electrolyte on the Zn anode.

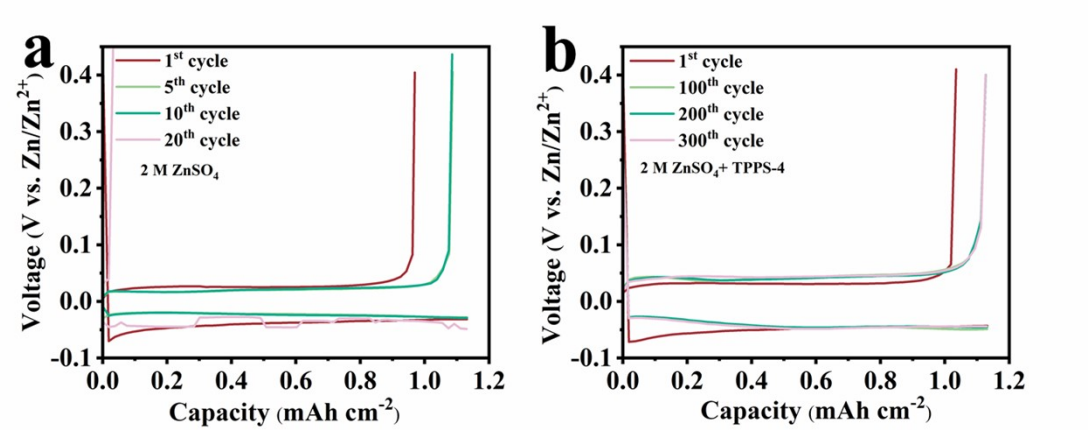

Fig. S10. Voltage profiles of Zn||Cu asymmetric cells in (a) 2 M $ZnSO_4$ and (b) 2 M $ZnSO_4$ + TPPS-4.

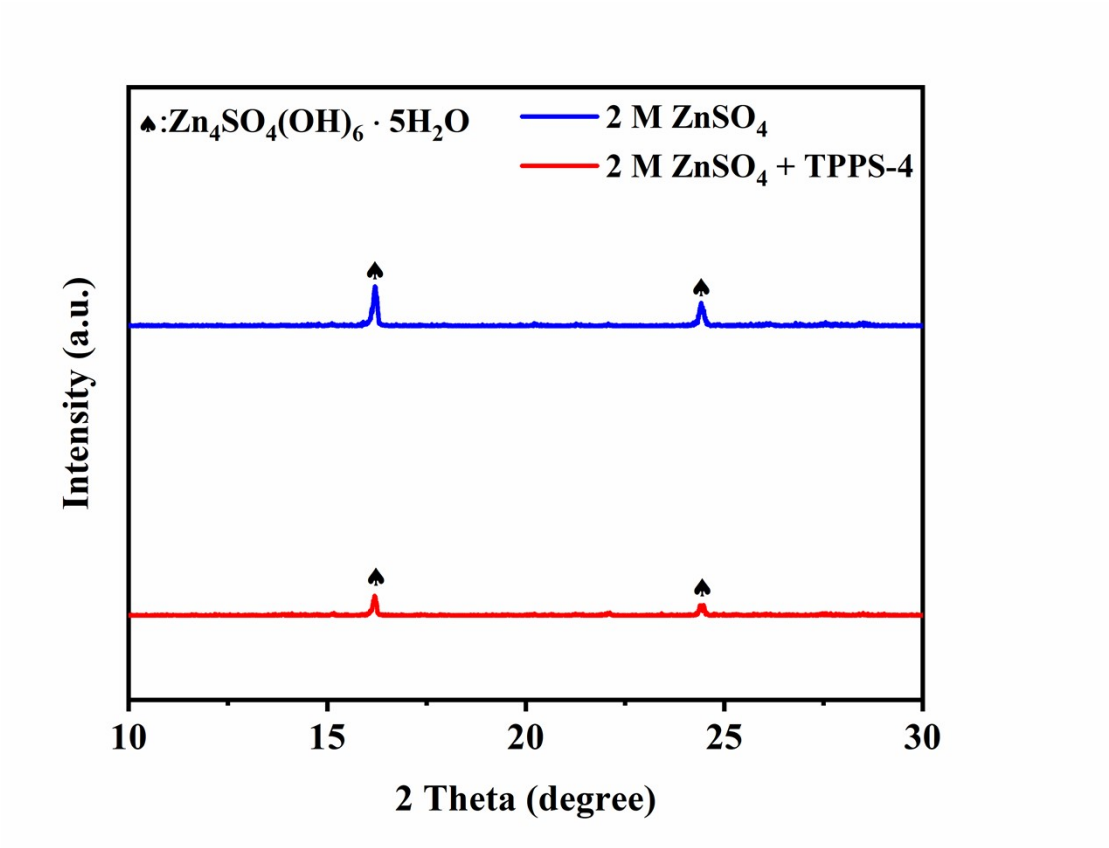

Fig. S11. XRD patterns of Zn anode after immersing in electrolytes without/with TPPS for 7 days.

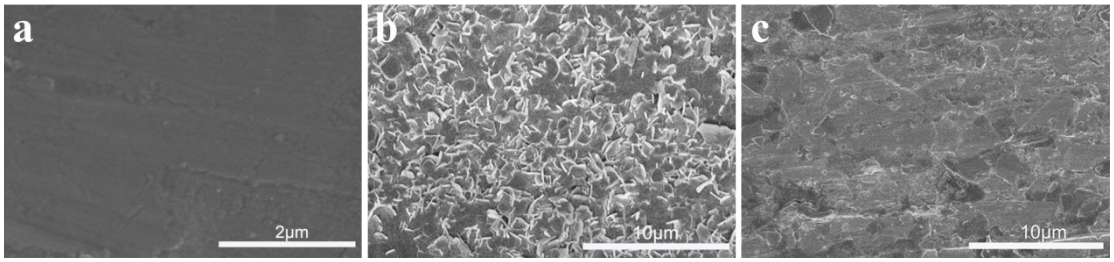

Fig. S12. SEM images of (a) Zn foil and Zn foil after immersing in (b) 2 M $ZnSO_4$ and (c) 2 M $ZnSO_4$ + TPPS-4 for 7 days.

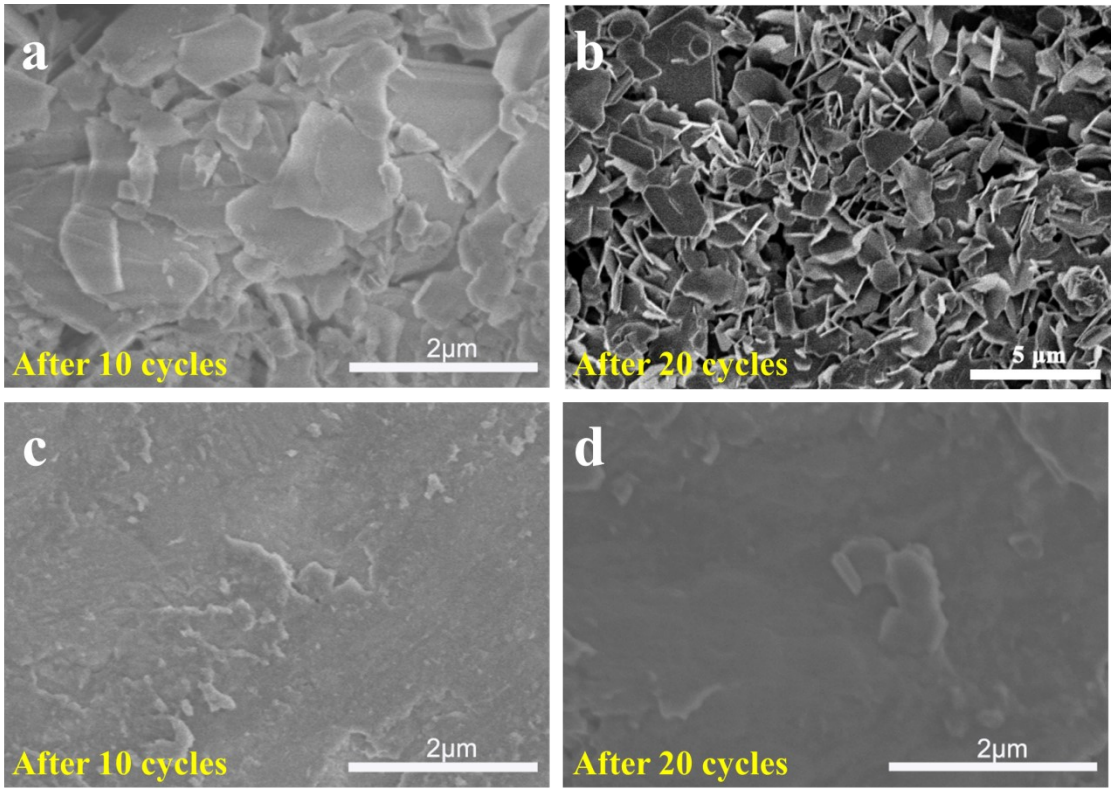

Fig. S13. SEM images of the nucleation and deposition behaviour of Zn^{2+}. (a, b) 2 M $ZnSO_4$. (c, d) 2 M $ZnSO_4$ + TPPS-4.

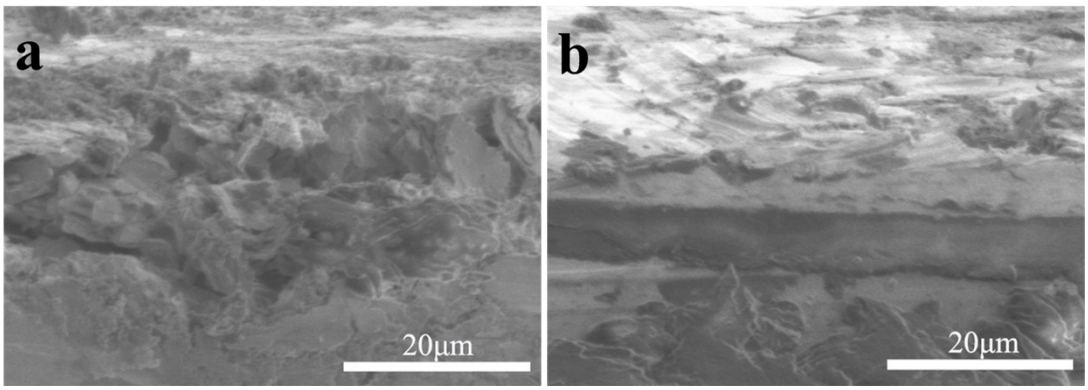

Fig. S14. Cross-section SEM images of the Zn anode in the (a) 2 M $ZnSO_4$ and (b) 2 M $ZnSO_4$ + TPPS-4.

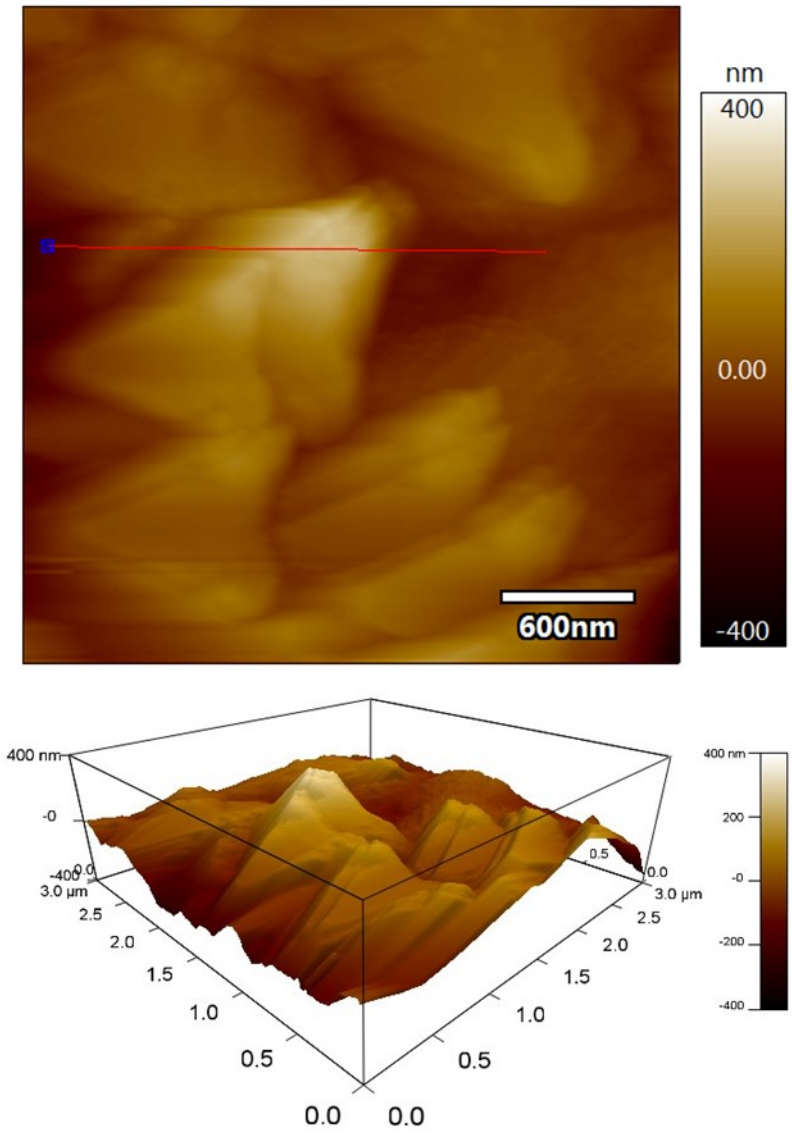

Fig. S15. AFM images of Zn anode in 2 M $ZnSO_4$.

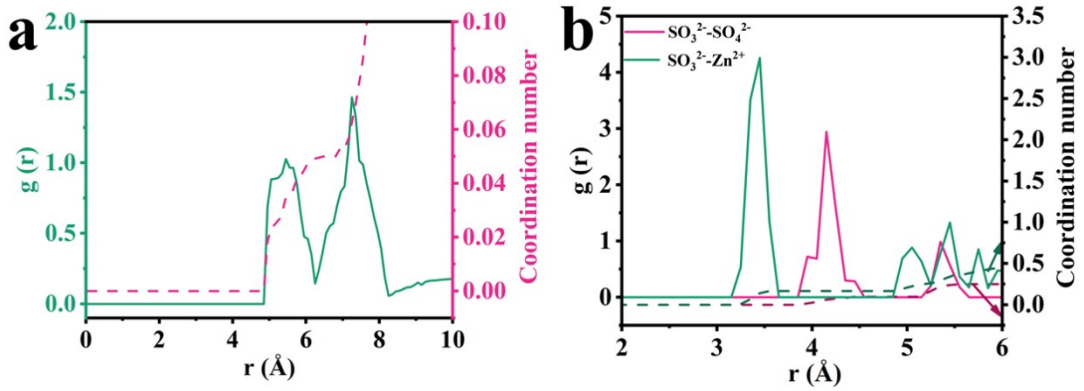

Fig. S16. RDFs of (a) Zn^{2+}-TPPS and (b) SO_3^{2-}-SO_4^{2-}/Zn^{2+} in 2 M $ZnSO_4$ + TPPS-4.

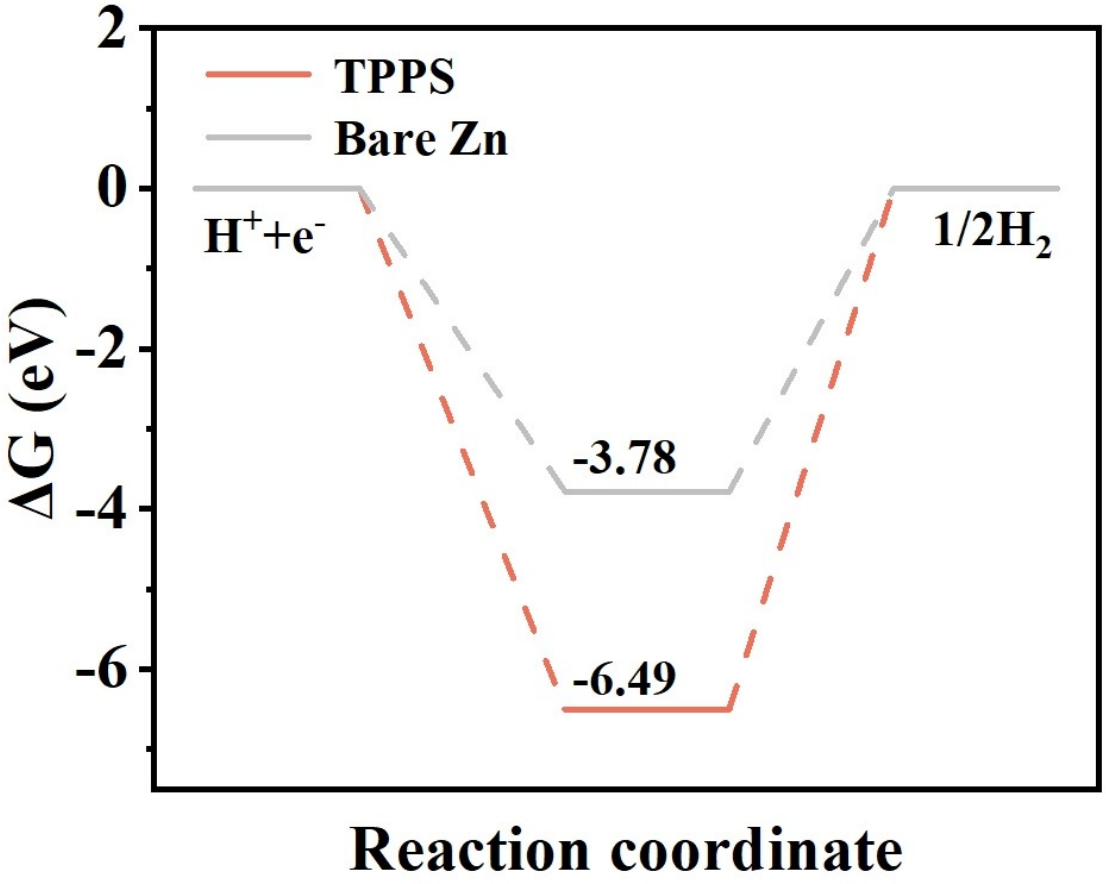

Fig. S17. Hydrogen adsorption Gibbs free energy (ΔGH) of Zn and TPPS.

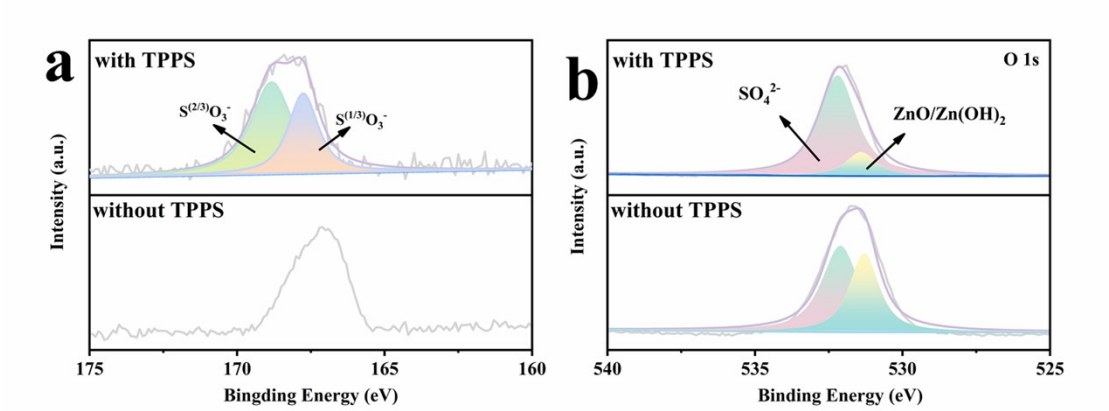

Fig. S18. (a) S2p and (b) O1s XPS spectra of Zn anode after cycling in 2 M $ZnSO_4$ and 2 M $ZnSO_4$ + TPPS-4.

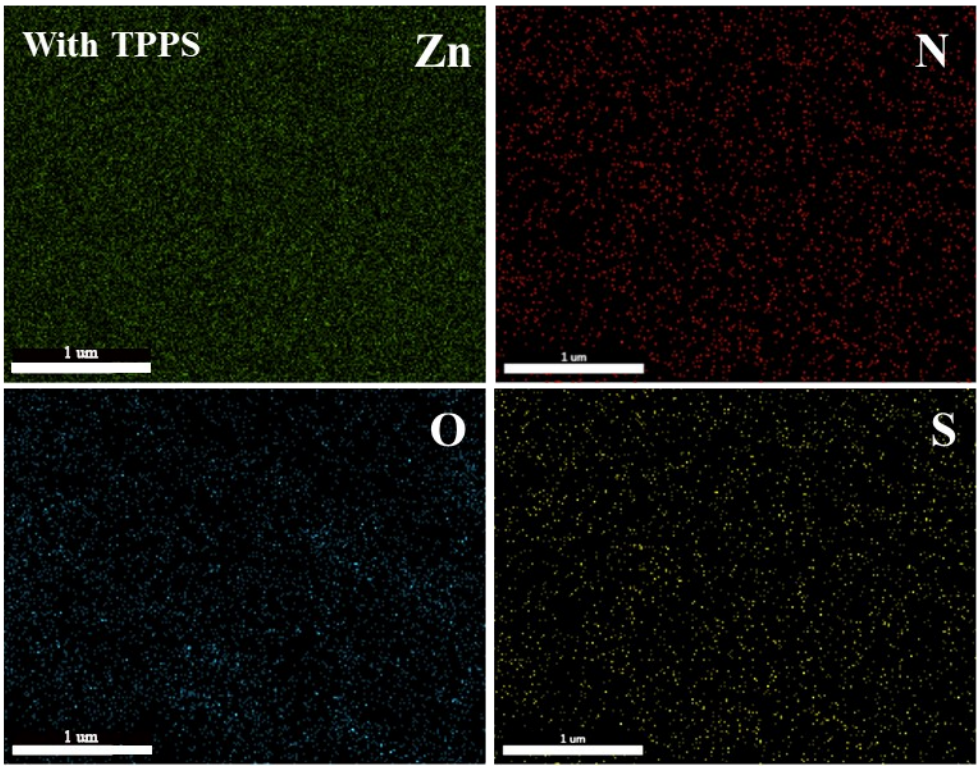

Fig. S19. EDS elemental mapping images of Zn anode in 2 M $ZnSO_4$ + TPPS-4.

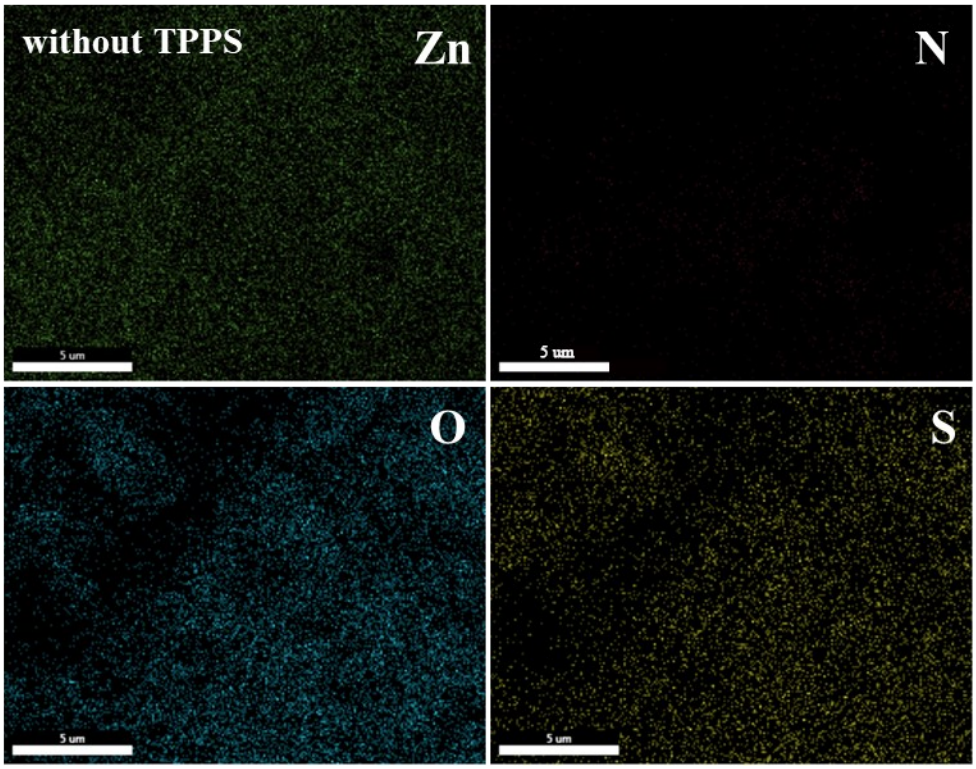

Fig. S20. EDS elemental mapping images of Zn anode in 2 M $ZnSO_4$.

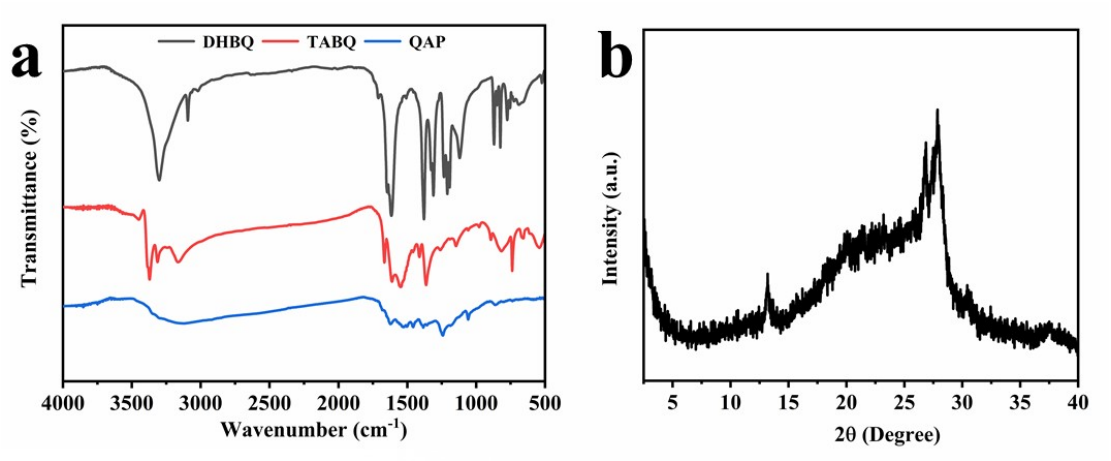

Fig. S21. (a) FT-IR spectra of DHBQ, TABQ and QAP. (b) PXRD pattern of QAP.

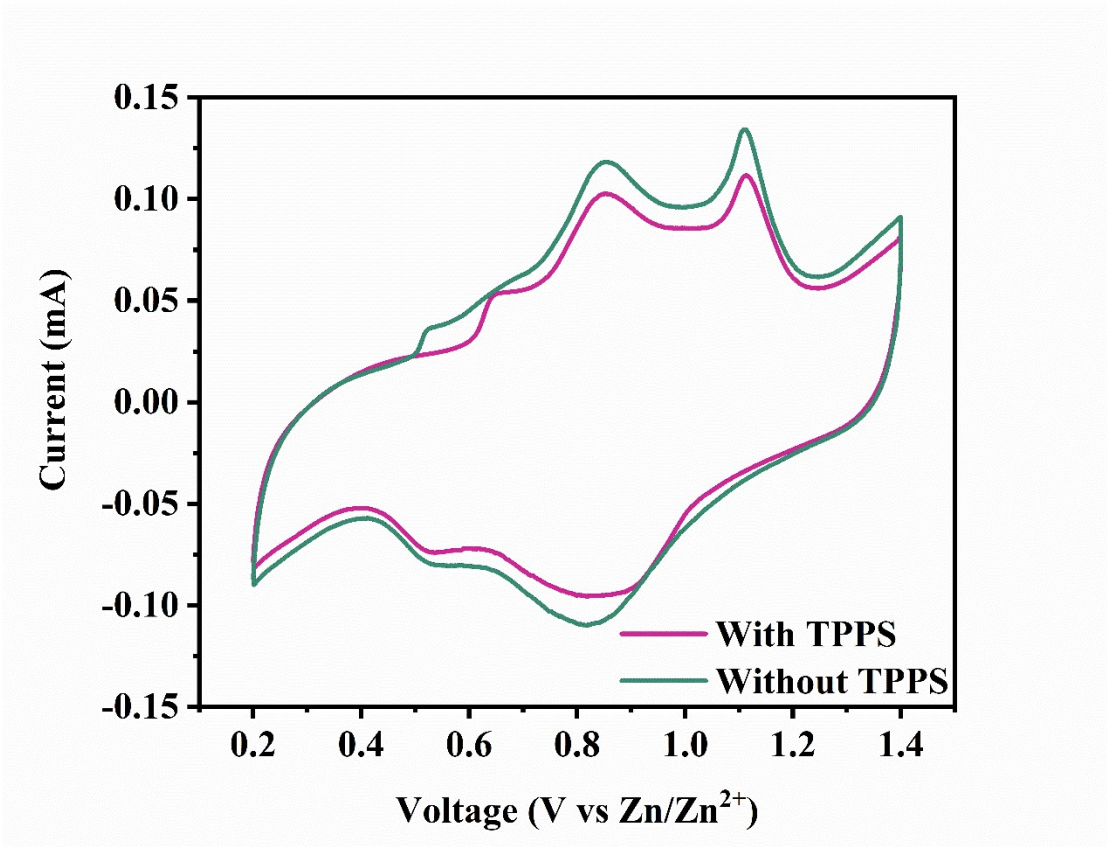

Fig. S22. CV curves of Zn||QAP full cell with different electrolytes.

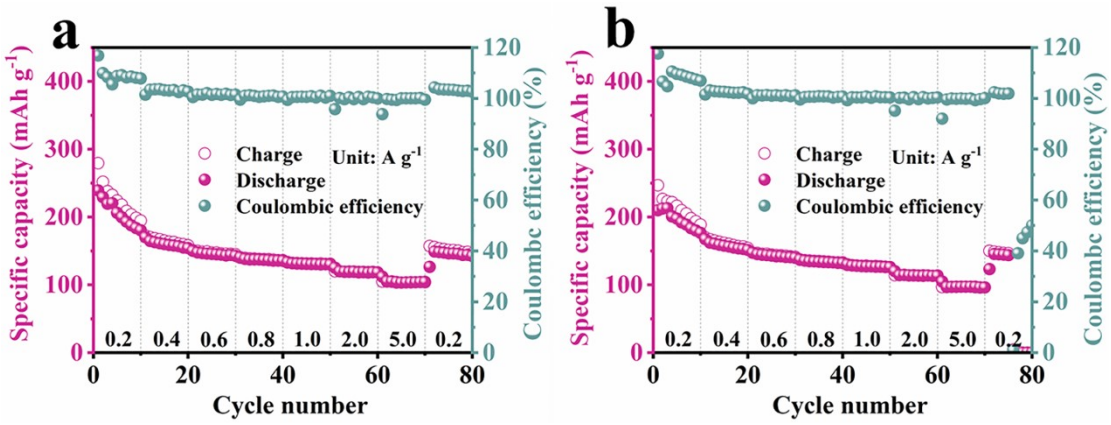

Fig. S23. Rate performance of Zn||QAP full cell in (a) 2 M $ZnSO_4$ + TPPS-4 and (b) 2 M $ZnSO_4$.

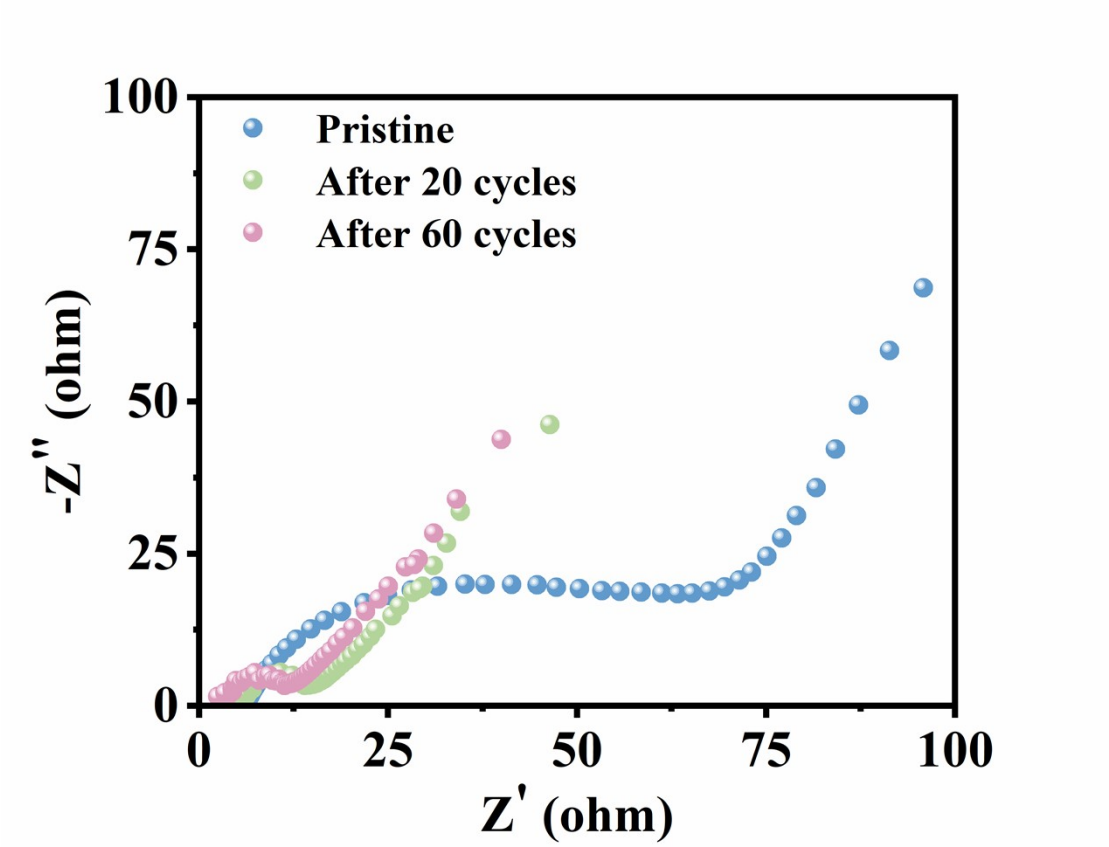

Fig. S24. EIS profiles of Zn||QAP full cell in 2 M $ZnSO_4$ + TPPS-4 before and after cycling.

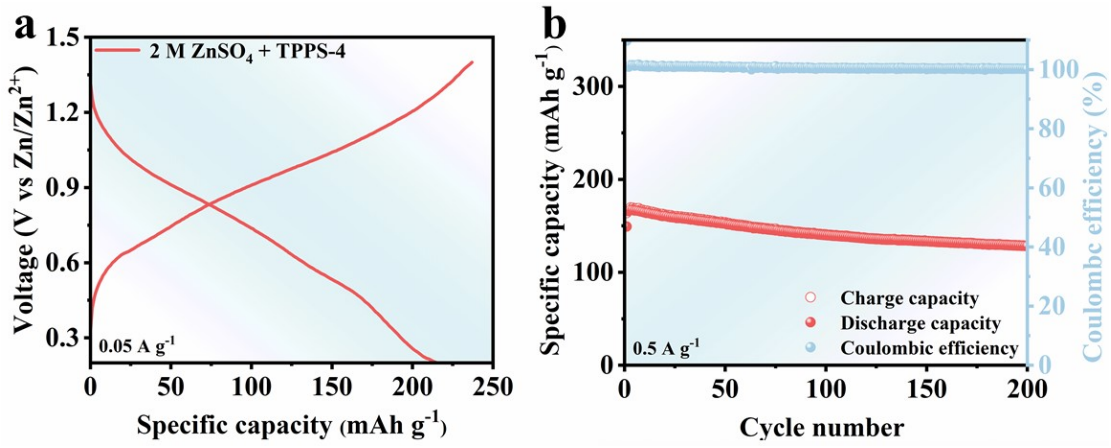

Fig. S25. (a) GCD profiles at 0.05 A g^{-1} and (b) long-term cycling stability at 0.5 A g^{-1} of Zn||QAP full cell at -10 ℃.

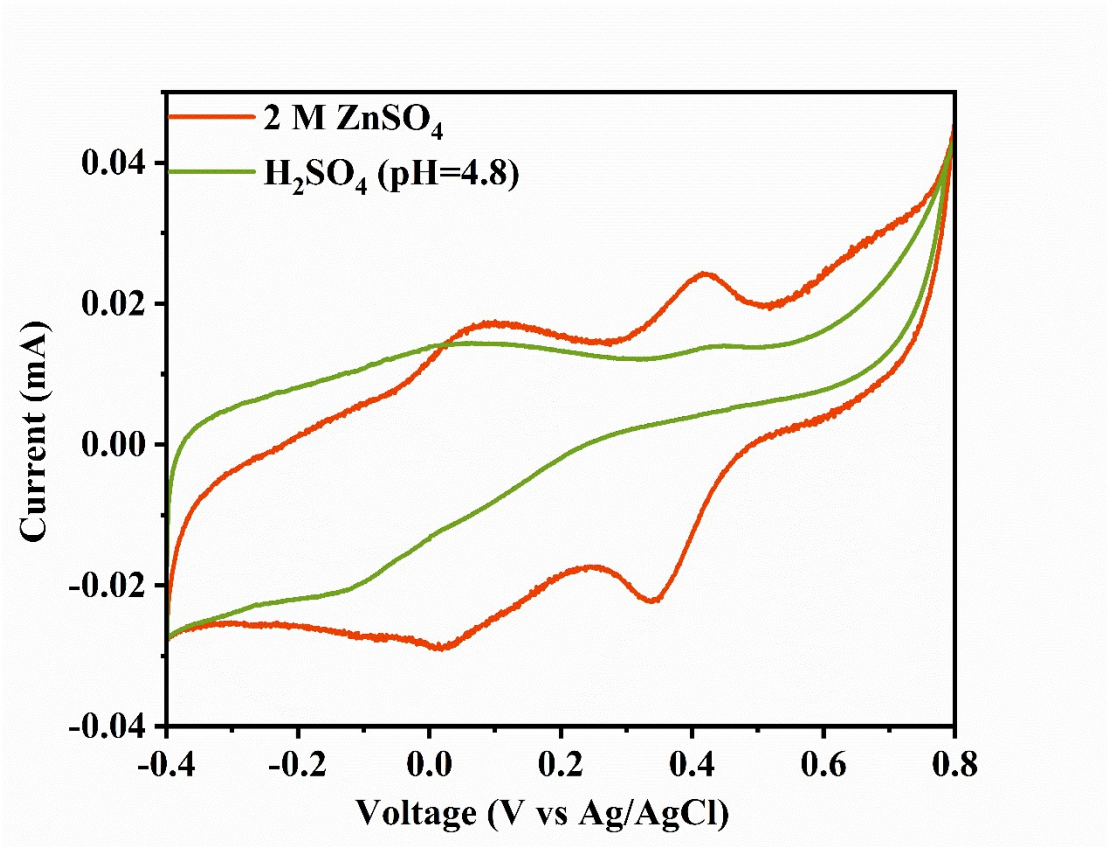

Fig. S26. CV curves of Zn||QAP full cell with different electrolytes.

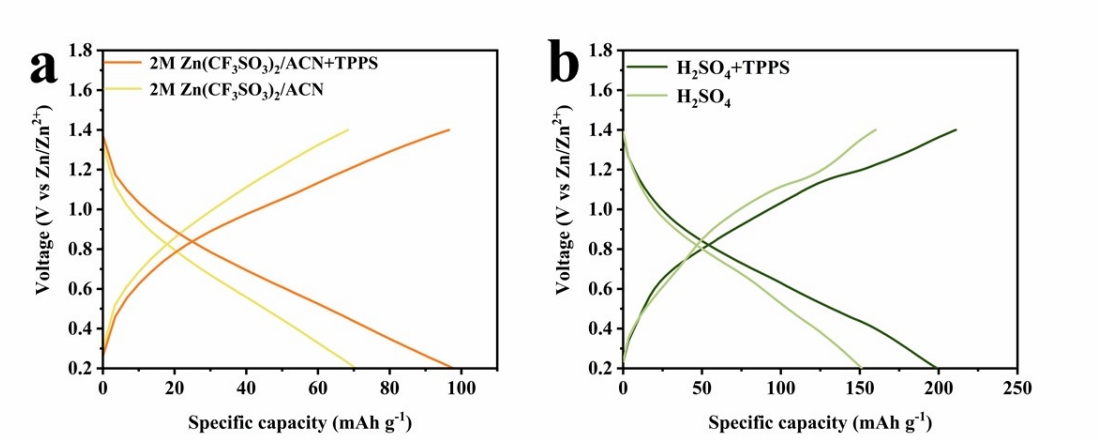

Fig. S27. GCD profiles of Zn||QAP full cell with different electrolytes.

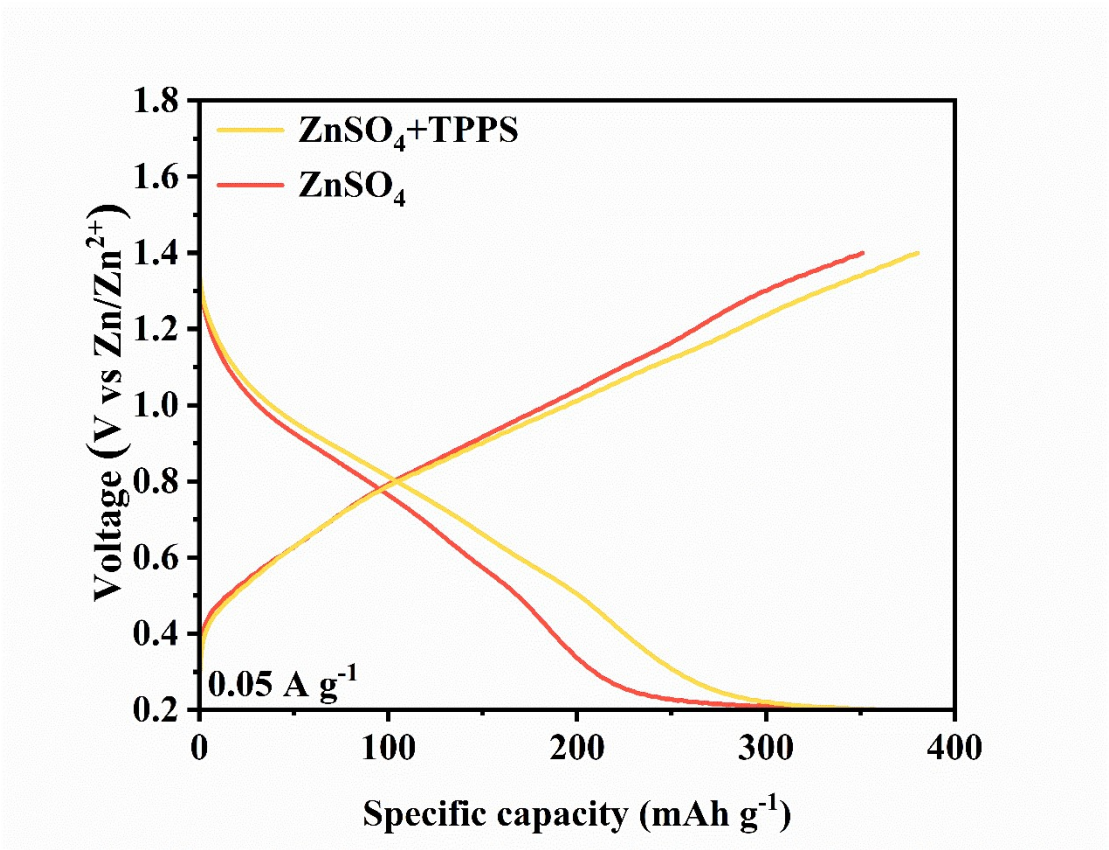

Fig. S28. GCD profiles of Zn||QAP full cell with different electrolytes.

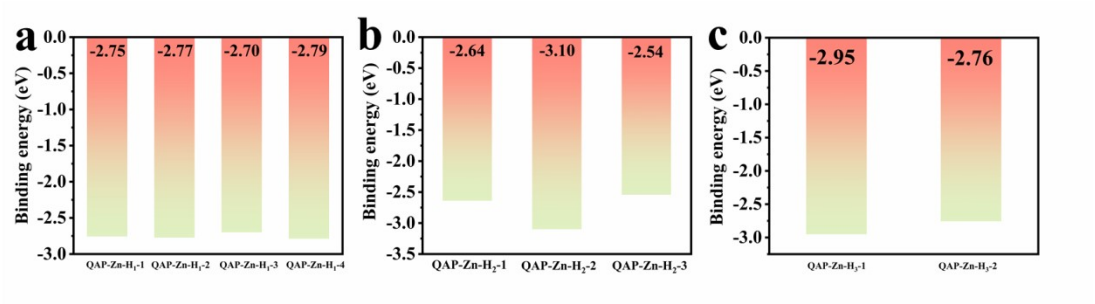

Fig. S29. Binding energies of QAP-Zn-H_1, QAP-Zn-H_2 and QAP-Zn-H_3 with different structures.

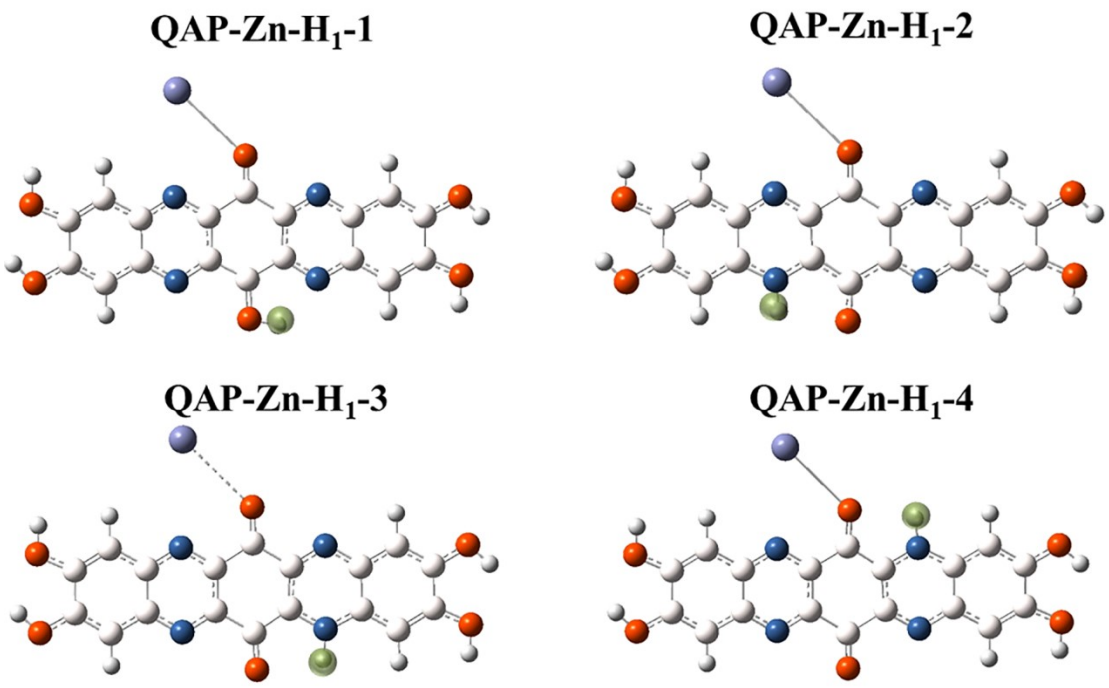

Fig. S30. The structures evolution of QAP-Zn-H_1.

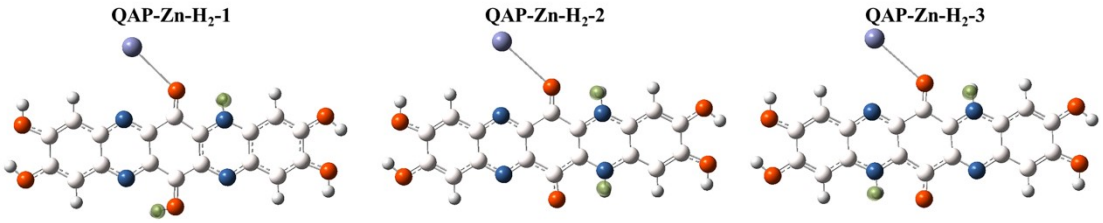

Fig. S31. The structures evolution of QAP-Zn-H_2.

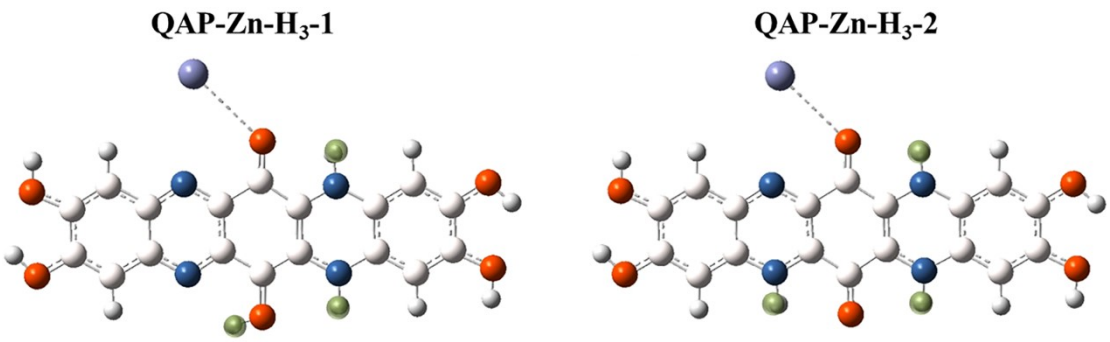

Fig. S32. The structures evolution of QAP-Zn-H_3.

Reference:

S1 R. Manivannan, S. Ciattini, L. Chelazzi and K. P. Elango, *RSC Adv.,* 2015, **5**, 87341.

S2 L. Cheng, J. Yu, L. Chen, J. Chu, J. Wang, H. G. Wang, D. Feng, F. Cui and G. Zhu, *Small,* 2023, **19**, 2301578.

S3 F. Weigend, Phys. *Chem. Chem. Phys.,* 2006, **8**, 1057.

S4 S. V. Sambasivarao and O. Acevedo, *J. Chem. Theory Comput.,* 2009, **5**, 1038.

S5 W. L. Jorgensen and J. Tirado-Rives, *Proc. Natl. Acad. Sci.,* 2005, **102**, 6665.

S6 G. Kresse and J. Furthmüller, *Comput. Mater. Sci*., 1996, **6**, 15.

S7 G. Kresse and J. Furthmüller, *Phys. Rev. B,* 1996, **54**, 11169.

S8 J. P. Perdew, K. Burke and M. Ernzerho, *Phys. Rev. Lett.,* 1996, **77**, 3865.

S9 G. Kresse and D. Joubert, *Phys. Rev. B,* 1999, **59**, 1758.

S10 P. E. Blöchl, *Phys. Rev. B,* 1994, **50**, 17953.

S11 S. Grimme, J. Antony, S. Ehrlich and H. Krieg, *J. Chem. Phys.,* 2010, **132**, 154104.

S12 H. J. Monkhorst and J. D. Pack, *Phys. Rev. B,* 1976, **13**, 5188.

S13 K. Mathew, R. Sundararaman, K. Letchworth-Weaver, T. A. Arias and R. G. Hennig, *J. Chem. Phys.,* 2014, **140**, 84106.

S14 K. Mathew, V. S. C. Kolluru and S. Mula, *J. Chem. Phys.,* 2019, **151**, 234101.